Active Control of Radiated Sound from Stiffened Plates Using IDE-PFC Actuators

Atanu Sahu

Institute of Composite Structures and Adaptive Systems, DLR, 38108 Braunschweig, Germany

Tirtha Banerjee, Arup Guha Niyogi and Partha Bhattacharya

Department of Civil Engineering, Jadavpur University, Kolkata -700032, India

(Received 29 November 2011; revised 7 January 2013; accepted 6 March 2013)

It has been a practice in modern day aircraft and automobile industries to manufacture a stiffened structure for significantly enhancing efficiency and strength without incurring a considerable weight increase. In the present study, an attempt is made to understand the effect of stiffeners on the sound radiation pattern of a vibrating plate. Subsequently, a velocity feedback control algorithm based on Linear Quadratic Regulator (LQR) methodology is developed to attenuate the radiated sound power from the vibrating structures with surface bonded piezo fibre composite (PFC) patches with interdigitated electrodes (IDE) as actuators and polyvinylidene fluoride (PVDF) films as sensors. Results are obtained for different orientations of stiffeners and various locations of PFC patches and are discussed.

NOMENCLATURE

ω	Natural frequency
$\widehat{\sigma}$	Radiation efficiency
$\{\sigma\}$	Stress vector
$\{\varepsilon\}$	Strain vector
{E}	Electric field vector
E	Young's modulus
ν	Poisson's ratio
ρ	Material density
[Q]	Elastic moduli matrix
{D}	Electrical displacement vector
[e]	Piezoelectric stress/charge constant
$[\varkappa]$	Electric permittivity or dielectric matrix
$[\varrho]$	Inertia matrix
[N]	Shape function matrix
$\{d\}$, $\left\{\dot{d}\right\}$, $\left\{\ddot{d}\right\}$	Generalized displacement, velocity, and acceleration vector
[M]	Mass matrix
$[\mathrm{K_{UU}}]$	Mechanical stiffness matrix
$[\mathrm{K}_{u\phi}]$	Electro-mechanical coupling stiffness matrix
$[\mathrm{K}_{\phi\phi}]$	Electrical stiffness matrix
[Z]	Position matrix of the piezo patch
[B]	Strain-displacement matrix
$\hat{Q}$	Electrical charge
$\{\mathrm{F_{el}}\}$	Electrical load vector
$\{y\}$, $\{\dot{y}\}$, $\{\ddot{y}\}$	Displacement, velocity, and acceleration vector in modal level

1. INTRODUCTION

In the present day automobile and aerospace industry, the objective is to increase fuel efficiency without compromising structural stiffness and strength. To achieve these objectives, the present trend is to use lightweight structural elements. However, these forms of structures have the possibility of generating unacceptable levels of sound and noise due to vibration. Since interior noise has a strong effect on passenger comfort and acceptance of the vehicle, researchers and engineers are continually working on different methodologies to reduce the noise level.

Classically, sound attenuation in the medium to high frequency acoustic range can be achieved in a passive manner by adding sound absorbing materials to the surface of the radiating structure. An alternate methodology is to use destructive interference in the sound source path. A more advanced form of the sound control is based on altering the vibrations of the noisy structure such that it radiates less sound. This alteration may be achieved by introducing discrete and collocated sensors and actuator pairs that fall under the scope of active control strategy.

The acoustic radiation problem has been addressed by various researchers, including Gladwell,[1] Gladwell and Zimmerman,[2] Seybert et al.,[3] and others. Cunefare has shown that the radiated sound power can be expressed in terms of acoustic radiation filters, surface radiation modes, and discrete surface velocities of the vibrating structure.[4] Elliot and Johnson compared two different formulations for calculating the acoustic power radiated from a vibrating structure in the free field and then implemented a feed forward control of sound power for a baffled square panel.[5] Radiation efficiencies and singular velocity patterns were introduced by Borgiotti and Jones using the singular value decomposition (SVD) of a radiation resistance matrix.[6] Gibbs et al. developed a radiation modal expansion (RME) technique to reduce computational effort and then apply a feedback control strategy with radiation filters employing multiple input or output smart sensor-actuators.[7] Bhattacharya et al. have shown that the size and geometry of the vibrating structure influences the cut-off limit of the acoustic ra-

diation filters.[8] In the paper by Liu et al., laboratory tests were performed to validate the theoretical prediction of the sound insulation properties of aircraft panels with ring frames and stringers.[9] They used shell panels made of both isotropic as well as composite materials. Engels et al. discussed the performances of different feedback controllers implemented on a plate structure using collocated velocity sensors and force actuators with the objective to minimize the kinetic energy and the radiated sound power.[10] In a review paper by Fuller, different methodologies for controlling the radiated sound from a vibratory structure were discussed—e.g., active acoustic control, active structural control, active structural-acoustic control with the help of point acoustic sources, smart foam as active skins, piezoelectric actuator-sensor pairs, etc.[11]

In the present work, an attempt is made to numerically model and estimate the radiated sound power in the free field from flat vibrating panels subjected to external disturbances. Subsequently, the formulation is extended for stiffened plates with stiffeners placed and oriented in different directions and positions. The study also aims to develop an active control strategy based on LQR methodology to minimize the sound radiating into the free field where the sensor voltage corresponding to the structural velocity is fed back into the piezo fibre composite actuator patches. For the structural analysis, a four node isoparametric quadrilateral finite element, with five mechanical degrees of freedom (3 translational and 2 rotational) per node based on first-order shear deformation theory is employed. Necessary transformation is used to incorporate the stiffeners into the FE model. A pair of electrical voltages, namely sensor voltage (ϕ^s) and actuator voltage (ϕ^a), are considered as additional degree of freedom applied per element containing piezo electric patches.

2. MATHEMATICAL FORMULATION

In this section, the mathematical formulation to describe the radiated acoustic power from planar baffled structures with and without stiffeners is presented. Thereafter, a feedback control algorithm based on LQR methodology with structurally bonded piezoelectric sensor and actuator devices is formulated and presented.

2.1. Acoustic

A vibrating structure consisting of an infinite number of natural mode shapes surrounded by an acoustic medium causes pressure perturbation in the medium that is experienced as sound. However, the structural mode shapes do not radiate independently and the inter-modal coupling between structural modes affects the radiated sound power. Therefore, reducing dominant structural modes may have little effect on the radiated power. Hence, it is important to develop acoustic radiation filters apart from identifying structural mode shapes. Acoustic radiation filters describe the radiated power in terms of discrete surface velocities and the surface radiation resistance, as shown by Cunefare.[4]

In the present analysis, the vibrating structure consists of a flat plate with and without stiffeners radiating sound into a free field. The plate is partitioned into N — numbers of equally sized rectangular elements with the size very small as compared to the acoustic wave length under consideration. Individual elements can be assumed as a point source placed in a baffle, and following the developments by Fahy and Gardonio,[12] the pressure at any observation point in the field can be expressed in the form of the Rayleigh integral for the acoustic Helmholtz equation. The Rayleigh integral is

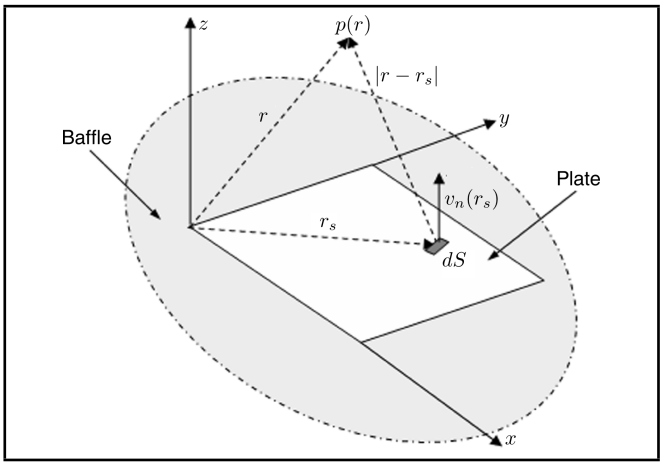

Figure 1. Schematic showing the baffled plate with the geometric interpretation of the Reyleigh integral.

$$p(r) = \frac{i\omega\rho_0}{2\pi}\int_S v_n(r_s)\frac{e^{-ik|r-r_s|}}{|r-r_s|}dS; \tag{1}$$

where $p(r)$ is the complex acoustic pressure amplitude at any location r, $k = \omega/c_0$ is the acoustic wave number with c_0 the speed of sound in the medium, and ϱ_0 is the density of the medium. The surface normal velocity is $v_n(r_s)$ on the vibrating source with a closed boundary S, as shown in Fig. (1). The sound power generated is equal to the surface integral of the normal component of the sound intensity

$$W = \frac{1}{2}\mathrm{Re}\left(\oint_S p(r_s)v_n^*(r_s)dS\right). \tag{2}$$

The Rayleigh integral is solved with the help of a numerical scheme. It is assumed that the normal velocity is constant across each element. That makes each element behave like an elemental radiator or piston that moves with constant harmonic velocity. For this discretization, the Rayleigh integral can also be written as

$$\mathbf{p_f} = \mathbf{Z_f}\mathbf{v_n}; \tag{3}$$

where $\mathbf{p_f}$ is the vector with pressures in a set of field points, $\mathbf{v_n}$ is the vector with normal surface velocities of the elemental radiators, and $\mathbf{Z_f}$ is a frequency dependent transfer matrix, whose elements are given by

$$(\mathbf{Z_f})_{ij} = \frac{i\omega\rho_0 \mathrm{S_e}}{2\pi}\frac{e^{-ikr_{ij}}}{r_{ij}}. \tag{4}$$

$\mathrm{S_e}$ defines the area of the elemental radiator and r_{ij} is the distance between the field point i and surface point j ($r_{ij} = |r_i - r_j|$).

For the same discretization, the expression for the sound power reduces to the summation

$$W = \frac{\mathrm{S_e}}{2}\mathrm{Re}(\mathbf{v_n^H p}); \tag{5}$$

where $\mathbf{p}$ is the vector with surface pressures, evaluated at the same points on the surface as v_n. With the substitution of $\mathbf{p} = \mathbf{Z}\mathbf{v_n}$, the sound power W can be obtained in terms of a discrete number of velocity measurements as

$$W = \mathbf{v_n^H R v_n}. \tag{6}$$

In this equation, $\mathbf{R} = (\mathrm{S_e}/2)\mathrm{Re}(\mathbf{Z})$ is called the radiation resistance matrix. This matrix $\mathbf{R}$ can be written as

$$\mathbf{R} = \frac{\omega^2 \rho_0 \mathrm{S_e^2}}{4\pi c_0} \begin{bmatrix} 1 & \frac{\sin(kr_{21})}{kr_{21}} & \dots & \frac{\sin(kr_{1N})}{kr_{1N}} \\ \frac{\sin(kr_{12})}{kr_{12}} & 1 & & \vdots \\ \vdots & & \ddots & \vdots \\ \frac{\sin(kr_{N1})}{kr_{N1}} & \dots & \cdots & 1 \end{bmatrix}.$$

Since $r_{ij} = r_{ji}$, the radiation resistance matrix $\mathbf{R}$ is symmetric and positive definite. The elements of the matrix depend on the properties of the acoustic medium, the frequency, and the geometry of the plate.

The radiation efficiency is defined as the ratio of the sound power radiated per unit area by the object to the sound power radiated by a reference source. The reference source is a baffled piston vibrating at a high frequency (wave number, $k\times$ area of the piston, $A \gg 1$) with a velocity equal to the space and time averaged, squared, normal velocity $\langle v_n^2 \rangle$ of the object. The radiation efficiency is given as

$$\widehat{\sigma} = \frac{W}{\rho_0 c_0 S \langle v_n^2 \rangle}; \tag{7}$$

where S is the total area of the object. The space and time averaged normal velocity is given by

$$\langle v_n^2 \rangle = \frac{1}{2S} \int_S |v_n(r_s)|^2 dS = \mathbf{v_n^H \dot{N} v_n}. \tag{8}$$

The radiation modes and the radiation efficiencies can be obtained by carrying out a singular value decomposition (SVD) on the matrix $\dot{\mathbf{N}}^{-1}\mathbf{R}$. As the radiation resistance matrix $\mathbf{R}$ depends upon the frequency, the SVD must be performed at all the frequency steps. As a result, both the radiation efficiency and the radiation mode shapes are functions of frequency. In order to predict the total power radiated over a certain frequency bandwidth, the characteristics of the $\mathbf{R}$ matrix are modelled over that bandwidth.

2.2. Constitutive Relationship

The structural form considered here consists of an isotropic stiffened plate with IDE-PFC patches bonded as actuators and piezo monolithic patches as sensors. The constitutive relationship for an isotropic material can be expressed as

$$\begin{Bmatrix} \sigma_{xx} \\ \sigma_{yy} \\ \tau_{yz} \\ \tau_{zx} \\ \tau_{xy} \end{Bmatrix} = \begin{bmatrix} \frac{E}{(1-\nu^2)} & \frac{E\nu}{(1-\nu^2)} & 0 & 0 & 0 \\ \frac{E\nu}{(1-\nu^2)} & \frac{E}{(1-\nu^2)} & 0 & 0 & 0 \\ 0 & 0 & \frac{E}{2(1+\nu)} & 0 & 0 \\ 0 & 0 & 0 & \frac{E}{2(1+\nu)} & 0 \\ 0 & 0 & 0 & 0 & \frac{E}{2(1+\nu)} \end{bmatrix} \begin{Bmatrix} \varepsilon_{xx} \\ \varepsilon_{yy} \\ \gamma_{yz} \\ \gamma_{zx} \\ \gamma_{xy} \end{Bmatrix}. \tag{9}$$

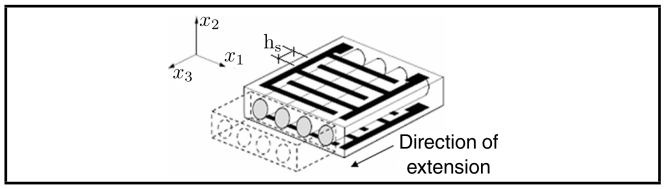

Figure 2. Actuation mechanism of piezo fiber composite (PFC) with interdigitated electrode (IDE).

In the case of piezo patches, the standard IEEE norm is followed and presented below as

$$\{\sigma\} = [\mathrm{Q}]\{\varepsilon\} - [\mathrm{e}]^{\mathrm{T}}\{\mathrm{E}\} \tag{10}$$

and

$$\{\mathrm{D}\} = [\mathrm{e}]\{\varepsilon\} + [\varkappa]\{\mathrm{E}\}; \tag{11}$$

where the notations have their usual meanings.

The electric field vector $\{\mathrm{E}\}$ is expressed as

$$\{\mathrm{E}\} = -\nabla\boldsymbol{\phi}; \tag{12}$$

where $\boldsymbol{\phi}$ is the applied electric potential.

In case of IDE-PFC patches (Fig. (2)), the electric field along the length of the patch between two consecutive electrode fingers is assumed to be linearly distributed with alternate electrodes being suitably grounded. There is a perfect bond between the piezo layer and the elastic substrate. Hence, the electric field for the actuator layer is expressed as

$$\mathrm{E^a} = -\frac{\phi^{\mathrm{a}}}{\mathrm{h}_s}; \tag{13}$$

where h_s is the distance between IDE.

In case of sensor elements, the electric field is assumed to be linearly distributed through the thickness of the piezo layer with the electrode in contact with the substrate being suitably grounded.

2.3. Finite Element Formulation

The governing equation for the structural motion is developed using the Hamiltonian formulation and is expressed as

$$\frac{d}{dt}\left(\frac{\partial T}{\partial \dot{q}_i'}\right) - \frac{\partial}{\partial q_i'}(T - U) = P_i; \tag{14}$$

where P_i is the generalized force and q_i' are the generalized coordinates.

The kinetic energy T is expressed as

$$T = \frac{1}{2}\int_V \{\dot{\mathrm{u}}\}^{\mathrm{T}}\{\rho\}\{\dot{\mathrm{u}}\}dv. \tag{15}$$

The potential energy U consists of potential due to mechanical strain U_{M} and electrical strain energy U_{E}, where U_{M} is given as

$$U_{\mathrm{M}} = \frac{1}{2}\int_V \{\varepsilon\}^{\mathrm{T}}\{\sigma\}\, dv. \tag{16}$$

With the inclusion of a piezoelectric patch as an actuator in the host structure, the potential energy due to the electric field needs to be taken care of in the potential energy term in Eq. (14) as:

$$U_{\mathrm{E}} = \frac{1}{2}\int_V \{\mathrm{E}\}\{\mathrm{D}\}\, dv. \tag{17}$$

The sensor is separately modelled and is explained in the next section.

The structure is discretized using a four-node isoparametric element. Five mechanical degrees of freedoms (3 translational and 2 rotational) are assumed per node. As already mentioned, one actuator voltage per element is incorporated in the FE model. The actuator modelling is done as per the work given in the paper by Azzouz et al.[13] Therefore, following the isoparametric concept, the mechanical degrees of freedom can be expressed in terms of the linear shape functions as

$$\{\mathrm{u}\} = [\mathrm{N}]\{d_e\}; \tag{18}$$

where $\{\mathrm{u}\}$ is the displacement vector at any point of the finite element and $\{d_e\}$ is the nodal displacement vector.

The finite element form of the governing equations of the system are written as

$$[\mathrm{M}]\left\{\ddot{d}\right\} + [\mathrm{K_{UU}}]\{d\} + [\mathrm{K_{U\phi}}]\{\phi^{\mathrm{a}}\} = \{\mathrm{F_m}\} \tag{19}$$

and

$$[\mathrm{K_{\phi U}}]\{d\} - [\mathrm{K_{\phi\phi}}]\{\phi^{\mathrm{a}}\} = \{\mathrm{F_{el}}\}; \tag{20}$$

where $\mathrm{F_m}$ is the mechanical load vector and
$[\mathrm{M}] = \int_A [\mathrm{N}]^{\mathrm{T}}[\rho][\mathrm{N}]dA$;
$[\mathrm{K_{UU}}] = \int_A [\mathrm{B}]^{\mathrm{T}}[\mathrm{D}][\mathrm{B}]dA$;
$[\mathrm{K_{\phi\phi}}] = \int_V \left(\frac{1}{\mathrm{h_s^2}}\right)[\mathrm{B_\phi}]^{\mathrm{T}}[\chi][\mathrm{B_\phi}]dV$; and
$[\mathrm{K_{U\phi}}] = \int_V \left(\frac{\mathrm{V_f}}{\mathrm{h_s}}\right)[\mathrm{B}]^{\mathrm{T}}[\mathrm{Z}]^{\mathrm{T}}[\mathrm{e}]^{\mathrm{T}}[\mathrm{B_\phi}]dV = [\mathrm{K_{\phi U}}]^{\mathrm{T}}$.

2.4. Sensor Modelling

The direct piezoelectric equation is used to calculate the output charge from the piezo sensors induced by mechanical strains. The electric displacement developed on the sensor surface is directly proportional to the mechanical strain acting on the sensor. By using a zero-input-impedance circuit, it is possible to show that the first term in the right-hand side of the piezoelectric constitutive Eq. (10) contributes less than the second term on the same side of the equation, and the second term in the right-hand side of the piezoelectric constitutive Eq. (11) is less significant than the first term on the same side of the equation. Thus, the sensor behaves like a pure current source. For such a configuration, the charge developed for the i^{th} sensor patch at location $z = h_{i+1}$ (distance from the mid-plane of the structure) can be expressed as

$$\hat{Q}_i(t) = \int_{A_i} D(x, y, h_{n+1}, t)\mathrm{dA}; \tag{21}$$

where $D(x, y, h_{n+1}, t) = [\mathrm{e}]^{\mathrm{T}}\{\varepsilon\}$ and $\{\varepsilon\} = [\mathrm{Z}][\mathrm{B}]\{\mathrm{d}_e\}$.

The sensor current is proportional to the rate of charge developed. Therefore,

$$i_{\text{sensor}} = \dot{\hat{Q}}; \tag{22}$$

and the sensor output voltage becomes

$$\phi^s = R_f i_{\text{sensor}} \tag{23}$$

or

$$\phi^s = R_f\,[\mathrm{K_s^e}]^{\mathrm{T}}\left\{\dot{d}_e\right\}; \tag{24}$$

where $[\mathrm{K_s^e}]^{\mathrm{T}} = \int_{A_i}[\mathrm{e}]^{\mathrm{T}}[\mathrm{Z}][\mathrm{B}]dA$ is called the sensor stiffness and R_f is the resistance offered by the piezo patch.

In the present formulation, the voltage produced in the sensor patches (Eq. (24)) mounted on the vibratory structure is fed back to the actuator patches after multiplying with the gain value $\mathbf{G}$ obtained from control law and thus the third term in Eq. (19) represents the equivalent piezoelectric load. Hence, the final governing equation takes the form

$$[\mathrm{M}]\left\{\ddot{d}\right\} + [\mathrm{K_{U\phi}}]\cdot\mathbf{G}\cdot[\mathrm{K}_s]^{\mathrm{T}}\{\dot{d}\} + [\mathrm{K_{UU}}]\{d\} = \{\mathrm{F_m}\}. \tag{25}$$

The final governing equation in the element level when assembled gives the global equation for the entire domain

$$[\mathrm{M_{gl}}]\left\{\ddot{d}_{\mathrm{gl}}\right\} + [\mathrm{C_{gl}}]\left\{\dot{d}_{\mathrm{gl}}\right\} + [\mathrm{K_{gl}}]\{d_{\mathrm{gl}}\} = \{\mathrm{F_{gl}}\}. \tag{26}$$

The FE model is developed in the MATLAB environment for response calculation and is simultaneously used to implement the control algorithm.

After carrying out the response analysis (Eq. (26)), one can obtain the surface velocities with and without the control voltages and obtain the radiated sound power from the vibrating plate from Eq. (6).

3. LQR CONTROL ALGORITHM

In the present section, the control algorithm implemented for the sound power reduction is discussed briefly. For the present study, a linear quadratic regulator (LQR) is considered, which is based on the quadratic performance index. The state-space model of the system in modal level is given by

$$\begin{Bmatrix}\dot{y}_i\\ \ddot{y}_i\end{Bmatrix} = \begin{bmatrix}0 & 1\\ -\omega_i^2 & 0\end{bmatrix}\begin{Bmatrix}y_i\\ \dot{y}_i\end{Bmatrix} + \begin{bmatrix}0\\ \hline -\mathrm{K_{U\phi}}\end{bmatrix}\{\phi^{\mathrm{a}}\},$$

$$i = 1, 2, 3 \text{ (number of modes considered)};$$

or

$$\dot{x} = \mathbf{A}x + \mathbf{B}\overline{u}. \tag{27}$$

The linear feedback control law for the system may be written as

$$\phi^{\mathrm{a}} = -\mathbf{G}\phi^s. \tag{28}$$

The elements of the gain matrix $\mathbf{G}$ are found by minimizing the performance index J,[14]

$$J = \int_0^\infty L(x, \overline{u})dt; \tag{29}$$

where L is a quadratic function of x and $\overline{u}$; the final form is expressed as follows:

$$J = \int_{t_0}^\infty (x^{\mathrm{T}}\mathbf{Q}_i x + \overline{u}^{\mathrm{T}}\mathbf{R}_i\overline{u})dt \tag{30}$$

$i = 1, 2, 3$ (number of modes considered).

Here, both $\mathbf{Q}$ and $\mathbf{R}$ matrices are real symmetric and $\mathbf{Q}$ consists of sensor stiffness at modal level while $\mathbf{R}$ can be chosen by the control designer. Again $\mathbf{Q}$ and $\mathbf{R}$ denote the relative importance of error and expenditure of control effort. The optimization of the performance index J results in the continuous time Riccati equation, which is solved in the MATLAB platform.

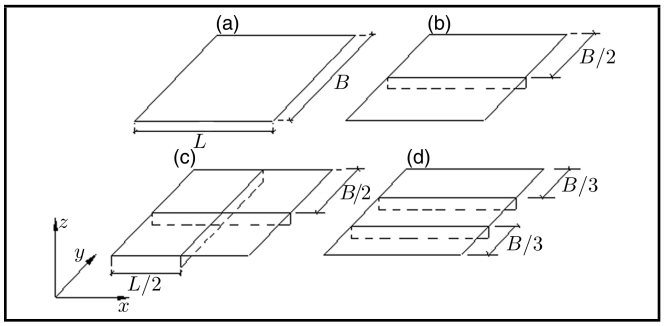

Figure 3. Schematic diagrams of unstiffened and stiffened plates.

4. RESULTS AND DISCUSSION

The present work on the behaviour of the vibrating structure on the radiated acoustic energy into the free field is carried out in two phases. The effect of the stiffeners on the radiating sound energy from the simply supported plate structure subjected to external mechanical excitations is investigated in the first phase of the work. In the next phase, an active control methodology is implemented to attenuate the emitted energy in some selected cases. The different structural forms considered for the present study are presented below:

Case I: Simply-supported unstiffened plate (Fig. (3a));

Case II: Simply-supported stiffened plate with single unidirectional stiffener parallel to x-axis (Fig. (3b));

Case III: Simply-supported stiffened plate with bidirectional cross stiffeners (Fig. (3c));

Case IV: Simply-supported stiffened plate with double unidirectional stiffeners parallel to x-axis (Fig. (3d)).

A square aluminium plate of size $1.0\,\text{m} \times 1.0\,\text{m}$ with thickness $0.004\,\text{m}$ (Young's modulus, $E = 70.0\,\text{GPa}$, Poisson's ratio, $\nu = 0.3$ and density, $\rho = 2\,700\,\text{kg/m}^3$) is considered for the analysis. For a stiffened plate, the depth of the stiffener is taken as $0.1\,\text{m}$ with the thickness maintained the same as that for the plate. For validating the developed formulation, a free vibration study is carried out initially on a stiffened plate and is discussed in the next subsection.

4.1. Validation of the Stiffened Plate Formulation

Free vibration frequencies are obtained for a simply-supported stiffened plate with unidirectional stiffener (Case II) from the present finite element model and from the ANSYS ver. 11.0 model using the SHELL 63 element. They are presented in Table 1. The dimensions and the material properties for the structure are kept the same as mentioned in the previous section. The flat portion of the plate is discretized into a 20×20 FE mesh while the stiffener is discretized using a 20×2 mesh. From Table 1 it is observed that the natural frequencies obtained from the two models compare well.

As stated earlier, the objective of the present study is to obtain radiated acoustic power from the vibrating plates. To achieve this objective, initially a singular value decomposition (SVD) to obtain the eigenvalues and the associated eigenvectors is performed on the radiation resistance matrix $\mathbf{R}$, given in Eq. (6). Using the radiation modal expansion (RME) technique, as explained in Gibbs et al.,[7] with the cut-off frequency at $250\,\text{Hz}$, the radiation plots are obtained and presented in Fig. (4), which according to Gibbs et al.[7] are termed as the radiation efficiency plots. The eigenvectors represent the radiation mode shapes. It is important to note that the radiation resistance matrix is dependent only on the plate geometry and is independent of the boundary condition and structural stiffness. In the present study, for all the cases considered, the radiating surface has the same geometry, and hence obtaining the eigenvectors and singular values for one case is sufficient and is then used for all the cases. The obtained radiation efficiency plots with the radiation mode shapes are subsequently in conjunction with the structural velocities used to calculate the radiated energy (Eq. (6)). In the next sections, acoustic response results for various cases are obtained and discussed.

Table 1. Comparison of non-dimensional frequencies (λ_i) of an isotropic (aluminium) stiffened plate (Case II).

Mode Number	Present Finite Element Code (λ_i)	ANSYS (λ_i)
1	0.0092	0.0091
2	0.0125	0.0123
3	0.0148	0.0147

Note:$\lambda_i = \omega_i \sqrt{\frac{\rho(1-\nu^2)}{E}}$ [Niyogi et al.[15]]

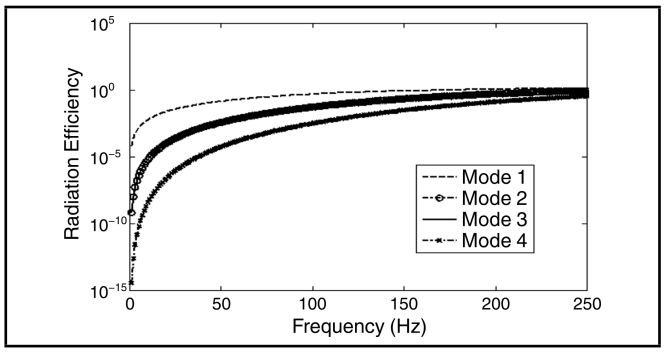

Figure 4. Radiation efficiency plots for the first 4 modes of the plate.

4.2. Radiated Acoustic Power from Unstiffened and Stiffened Plates

In the present section, radiated sound power from the four different types of vibrating structures (Case I to IV), due to the application of an external transient excitation of $1\,\text{kN}$, is obtained. The load (Fig. (5)) is applied for 0.01 seconds over an area of $0.05\,\text{m} \times 0.05\,\text{m}$ with the centre of the loading point located at $0.125\,\text{m}$ along the x- and y-axes from the origin of the global coordinate system (Fig. (3)). The radiated sound power, obtained using Eq. (7), is calculated as $\log_{10}\left(\frac{\widehat{\sigma}}{10^{-12}}\right)^{10}$ in dB and is plotted in Fig. (6).

It is observed from Fig. (6) that the reduction of radiated acoustic power in each mode is not assured with the addition of stiffeners. The sound power level increases for Case III as compared to Case I. For stiffened plates, the arrangement of the stiffener plays an important role in the reduction of the radiated sound power level. Though in both Case III and Case IV the number of stiffeners is the same, in Case IV the radiated power

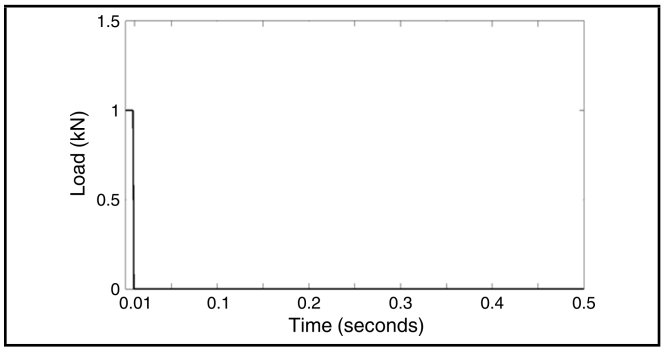

Figure 5. Transient load applied at $0.125\,\mathrm{m}$ along the x- and y-axes of plate structure.

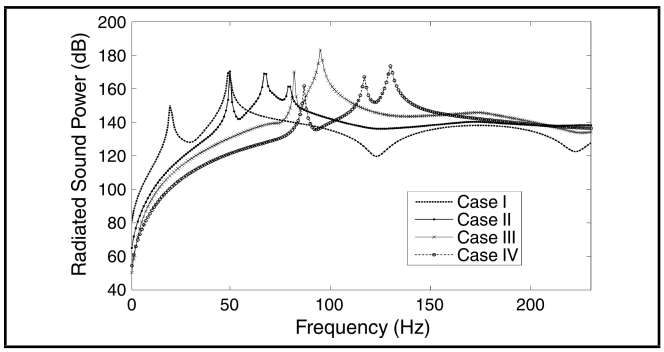

Figure 6. Radiated acoustic power of the stiffened plates (Case I to IV) subjected to a transient excitation of $1.0\,\mathrm{kN}$ (Fig. (5)).

is less in all the modes due to the arrangement of the stiffeners (Figs. (3c) and (3d)). It is also observed that with the addition of stiffeners the system frequency shifts; hence, the placing or arrangement of the stiffener needs some optimization study so that it does not interfere with the loading frequency. Moreover, stiffening the structure with the addition of a stiffener at any arbitrary position is not the sole solution to reduce the emitted acoustic energy, which necessitates the need for active control. Furthermore, the proper optimization technique should be implemented for the placement of stiffeners.

Additionally, the output to input pressure ratio (transmission ratio) is calculated for various cases and presented in Fig. (7). It is observed that the ratio is always less than 1. This suggests that only a part of the input energy is radiated as sound.

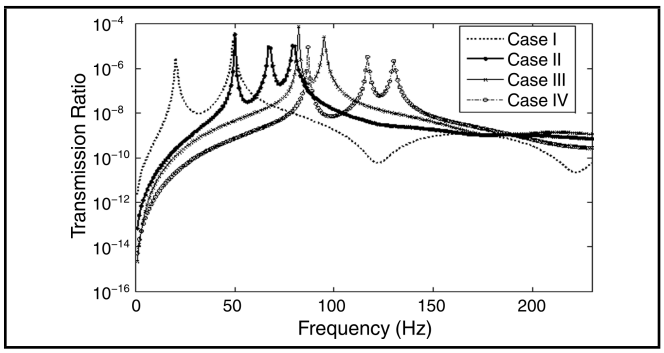

Figure 7. Output pressure to input pressure (transmission ratio) for the stiffened plates subjected to a transient excitation of $1.0\,\mathrm{kN}$ (Fig. (5)).

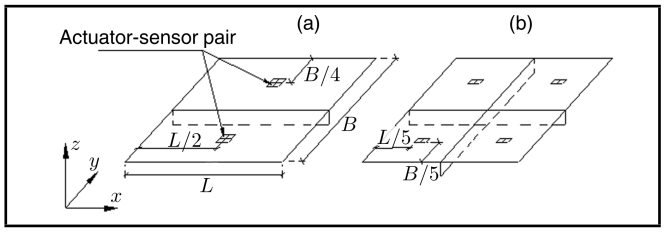

Figure 8. Piezoelectric patch locations for (a) a unidirectional and (b) a bidirectional stiffened plate.

Table 2. Mechanical and electrical properties of the actuator and sensor (Guennam and Luccioni,[16] and Liew et al.[17]

	IDE-PFC Actuator (PZT-5H)	PVDF Film Sensor
Geometric Properties		
Length, L	$0.05\,\mathrm{m}$	$0.05\,\mathrm{m}$
Width, B	$0.05\,\mathrm{m}$	$0.05\,\mathrm{m}$
Thickness	$0.001\,\mathrm{m}$	$40 \times 10^{-6}\,\mathrm{m}$
Elastic and Material Properties		
E	—	$2.0\,\mathrm{GPa}$
ν	—	0.28
ρ	$7740\,\mathrm{kg/m^3}$	$1800\,\mathrm{kg/m^3}$
Electrical Properties		
e_{22}	$22.9\,\mathrm{C/m^2}$	—
$\mathrm{e}_{31} = \mathrm{e}_{32}$	—	$0.046\,\mathrm{C/m^2}$
$\varkappa_{11} = \varkappa_{22}$	$1.27 \times 10^{-8}\,\mathrm{F\,m^{-1}}$	$106.2\,\mathrm{F\,m^{-1}}$
$\varkappa_{33}$	$1.51 \times 10^{-8}\,\mathrm{F\,m^{-1}}$	—

Note: Spacing of interdigitated electrode $\mathrm{h}_s = 0.0005\,\mathrm{m}$ and fibre volume fraction $V_f = 0.2$

4.3. Active Control of Radiated Acoustic Power

It is already seen in the earlier section that the attenuation of the acoustic energy is not always promised with the stiffening of the structure. Hence, a piezo-based active control strategy based on velocity feedback is attempted in the second phase. Piezo fibre composite with interdigitated electrode (IDE-PFC; PZT 5H) patches are used as actuators while PVDF films are employed as sensors for which the properties are mentioned in Tables 2 and 3.[16,17] Among the four cases (I to IV), studies have been conducted on two typical stiffened plates with unidirectional (Case II) and bidirectional stiffeners (Case III). Eight pairs of collocated actuator-sensor patches are mounted on the top of the stiffened plate. The schematic is shown in Fig. (8).

Prior to the control of radiated sound, the piezoelectric formulation is validated with standard data available in open literature and with the results obtained from ANSYS software. An IDE-PFC patch (PZT-5H) measuring $0.05\,\mathrm{m}$ long, $0.02\,\mathrm{m}$ wide, and having a thickness of $0.001\,\mathrm{m}$ with a fibre-volume ratio of unity, with a pair of electrodes placed at a distance of $0.05\,\mathrm{m}$ along the length, is modelled using the present FE formulation and in the ANSYS ver. 11.0 model using the SOLID 5 element. An electrical potential of unit (1) voltage is applied across the electrode. The longitudinal strain obtained from the ANSYS model is 0.350×10^{-8} and that from the present FE model is found to be $0.350\,69 \times 10^{-8}$, which compares extremely well. Moreover, the in-plane block force obtained from the actuator patch is calculated to be $0.4580\,\mathrm{N/m}$ which compares very well with the formulation given by Bent[18] in his work.

Table 3. Elastic Properties of the IDE-PFC actuator (PZT-5H) (Guennam and Luccioni[16])

Q_{11}	Q_{12}	Q_{22}	Q_{31}	Q_{32}	Q_{33}	Q_{44}	Q_{55}	Q_{66}
130.6	85.66	135.8	88.3	90.42	121.3	23.47	22.99	22.99

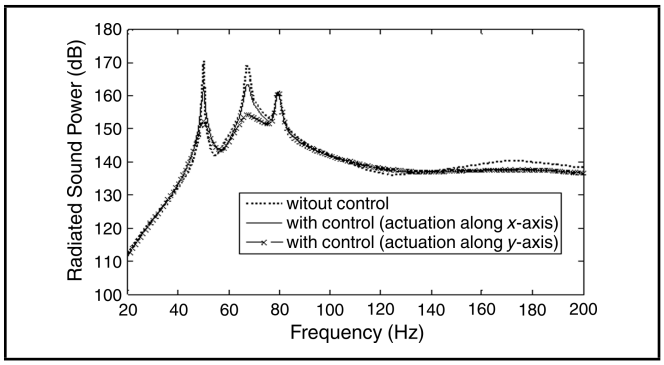

Figure 9. Radiated acoustic power (uncontrolled and controlled) from the stiffened plate with the unidirectional stiffener (Case II) subjected to a transient excitation of 1.0 kN (Fig. (5)).

4.4. Control of Radiated Acoustic Power from the Stiffened Plate with Unidirectional Stiffener (Case II)

As has been previously discussed in implementing the active control scheme, the sensor signals obtained from the vibrating structure are fed back to the actuator with proper feedback gains derived from the LQR algorithm. These gain values are obtained by minimizing J (Eq. (29)), which is again dependent on R (Eq. (30)). As R is correlated with expenditure of control effort, it is chosen in such a manner that the capacity of the actuator patches should not be exceeded. In the present study, two different principal orientations of the IDE-PFC actuators are considered—(i) along the x-axis and (ii) along the y-axis. The dimension, material properties, and the nature of the applied external loading are already mentioned in Section 4 and Section 4.2. The piezoelectric properties of the actuator and sensor are presented in Tables 2 and 3.

The plots of the uncontrolled and controlled sound power radiating into the free field are shown in Fig. (9). As observed in Fig. (9), the radiated sound power can be reduced significantly by considering the structural velocities, as only the feedback state which effectively increases the damping. Moreover, this active control scheme is capable of reducing the radiated energy, which is not always assured with the passive strategy like arbitrarily stiffening the structure. It is also seen that for the PFC actuators having their principal actuation direction along the x-axis, the reduction of radiated acoustic power in the free field is almost 7.7 dB for the first mode; whereas, for the same mode almost 18 dB reduction is achieved with the principal actuation direction along the y-axis. From the plot, it is clear that for the present structural configuration, the d_{22} actuation is much more pronounced in attenuating the radiated energy in the first and second modes when compared with the d_{11} actuation for the same control effort. In the first case, maximum voltage in the actuator patch is approximately 48 volts (peak to peak), whereas in the next case it is approximately 46 volts. It is imperative to note that in both cases, control in the third mode is not very effective, as the actuator patches lay on the inflexion line (Fig. (10)). Hence, it is evident from Fig. (10) (3rd mode of Case II) that the actuator patches are incapable of controlling the energy radiated in the third mode with the given actuator location.

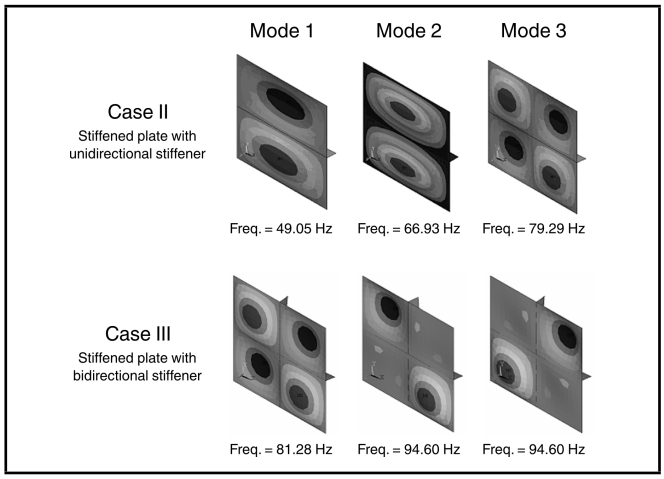

Figure 10. Mode shape plots for the stiffened plates (Case II and III).

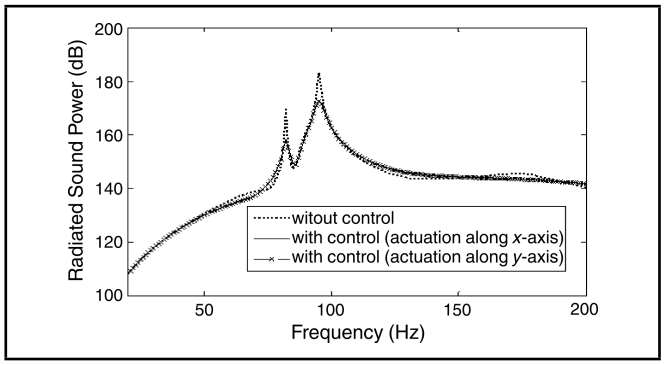

Figure 11. Radiated acoustic power (uncontrolled and controlled) from the stiffened plate with the bidirectional stiffener (Case III) subjected to a transient excitation of 1.0 kN (Fig. (5)).

4.5. Control of Radiated Acoustic Power from the Stiffened Plate with a Bidirectional Stiffener (Case III)

In the present section, the attempt is to reduce the free field sound power radiated from the bi-directionally stiffened plate (Case III) with the same number of actuator-sensor pairs (Fig. (8b)) as in the previous case, but with a different orientation of the patches. The results are plotted in Fig. (11).

In the first case, i.e., when the principal actuation direction is along the x-axis, a reduction of sound power amounting to 11.9 dB in the 1st mode and 10.5 dB in the 2nd mode is achieved with 43 volts as maximum input voltage to the actuator patch, but it reduces to 42 volts when the actuation direction is rotated by 90°. It is also seen that for d_{22} actuation, the reduction achieved in the two modes is 12 dB and 10.7 dB, respectively. Hence, it can be concluded that in this particular case the orientation of the patches does not have much influence, which is also shown in the mode shapes for this case (Fig. (10)).

5. CONCLUSION

In the present work, a study has been carried out on the sound radiation characteristics of the un-stiffened as well as the stiffened plates in the free field. As it is shown that arbitrarily stiffening the structure is not the sole solution to attenuating the radiated sound power, one should either go for optimizing the stiffener locations or implementing an active control scheme for a reasonable reduction in the radiated energy. In the present work, an active control scheme is implemented by providing sensor voltages as feedback signals multiplied with the proper gain values obtained from the LQR algorithm to the actuator patches collocated on the structure. Two cases have been considered to elucidate the effectiveness of the control algorithm; however, it is found that for maximum utilization of the active control system, an optimization study should be carried out for positioning the piezo patches. The work can be extended further to optimize the stiffener locations of the structure and also in optimizing the positions of actuator-sensor pairs towards achieving the maximum reduction in the radiated sound.

REFERENCES

[1] Gladwell, G. M. L. A finite element method for acoustics, *Proc. 5th International Congress on Acoustics*, Liège, Belgium, (1965).

[2] Gladwell, G. M. L. and Zimmerman, G. On the energy and complimentary energy formulations of acoustic and structural vibration problems, *J. Sound Vib.*, **3** (3), 233–241, (1966).

[3] Seybert, A. F., Soenarko, B., Rizzo, F. J., and Shippy, D. J. Application of the BIE method to sound radiation problems using an isoparametric element, *Trans. ASME, J. Vib., Acous., Stress and Reliability in Design*, **106** (3), 414–420, (1984).

[4] Cunefare, K. A. Effect of modal interaction on sound radiation from vibrating structures, *AIAA J.*, **30** (12), 2819–2828, (1992).

[5] Elliott, S. J. and Johnson, M. E. Radiation modes and the active control of sound power, *J. Acoust. Soc. Am.*, **94** (4), 2194–2204, (1993).

[6] Borgiotti, G. V. and Jones, K. E. Frequency independence property of radiation spatial filters, *J. Acoust. Soc. Am.*, **96** (6), 3516–3524, (1994).

[7] Gibbs, G. P., Clark, R. L., Cox, D. E., and Vipperman, J. S. Radiation modal expansion: application to active structural acoustic control, *J. Acoust. Soc. Am.*, **107** (1), 332–339, (2000).

[8] Bhattacharya, P., Rose, M., and Heintze, O. Active structural acoustic control of laminated plates using RME technique, *Proc. 9th International Conference on Vibrations Problems*, Kharagpur, India, (2009).

[9] Liu, B., Feng, L., and Nilsson, A. Sound transmission through curved aircraft panels with stringer and ring frame attachments, *J. Sound Vib.*, **300** (3-5), 949–973, (2007).

[10] Engels, W. P., Baumann, O. N., Elliot, S. J., and Fraanje, R. Centralized and decentralized control of structural vibration and sound radiation, *J. Acoust. Soc. Am.*, **119** (3), 1487–1495, (2006).

[11] Fuller, C. R. Active control of sound radiation from structures: progress and future directions, *Active 2002*, Southampton, United Kingdom, (2002).

[12] Fahy, F. and Gardonio, P. *Sound and structural vibration: radiation, transmission and response*, Oxford University Press, Oxford, United Kingdom, (2007), 2nd Ed.

[13] Azzouz, M. S., Mei, C., Bevan, J. S., and Ro, J. J. Finite element modeling of MFC/AFC actuators and performance of MFC, *J. Intel. Mat. Syst. Str.*, **12** (9), 601–612, (2001).

[14] Ogata, K. *Modern control engineering*, Prentice-Hall, India, (1998), 3rd Ed.

[15] Guha Niyogi, A., Laha, M. K., and Sinha, P. K. Finite element vibration analysis of laminated composite folded plate structures, *Shock Vib.*, **6** (5-6), 273–283, (1999).

[16] Guennam, A. E. and Luccioni, B. M. FE modeling of a closed box beam with piezoelectric fiber composite patches, *Smart Mater. Struct.*, **15** (6), 1605–1615, (2006).

[17] Liew, K. M., He, X. Q., Tan, M. J., and Lim, H. K. Dynamic analysis of laminated composite plates with piezoelectric sensor/actuator patches using the FSDT mesh-free method, *Int. J. Mech. Sci.*, **46** (3), 411–431, (2004).

[18] Bent, A.A. PhD Thesis, MIT, Active fiber composites for structural actuation, Cambridge, Massachusetts, (1997).